Role of Kinetic Instability in Runaway-Electron Avalanches and Elevated Critical Electric Fields

Chang Liu, Eero Hirvijoki, Guo-Yong Fu, Dylan P. Brennan, Amitava Bhattacharjee, and Carlos Paz-Soldan

Phys. Rev. Lett. **120**, 265001 — Published 28 June 2018

DOI: 10.1103/PhysRevLett.120.265001

Role of kinetic instability in runaway electron avalanche and elevated critical electric fields

Chang Liu,[1] Eero Hirvijoki,[1] Guo-Yong Fu,[2,1] Dylan P. Brennan,[3] Amitava Bhattacharjee,[1,3] and Carlos Paz-Soldan[4]

[1]*Princeton Plasma Physics Laboratory, Princeton, New Jersey 08540, USA*

[2]*Zhejiang University, Hangzhou, Zhejiang, 310027, China*

[3]*Princeton University, Princeton, New Jersey 08544, USA*

[4]*General Atomics, San Diego, California 92186, USA*

(Dated: May 29, 2018)

Abstract

The effects of kinetic whistler-wave instabilities on the runaway-electron (RE) avalanche is investigated. With parameters from DIII-D experiments, we show that RE scattering from excited whistler waves can explain several poorly understood experimental results. We find an enhancement of RE avalanche for low density and high electric field, but for high density and low electric field the scattering can suppress the avalanche and raise the threshold electric field, bringing the present model much closer to observations. The excitation of kinetic instabilities and the scattering of resonant electrons are calculated self-consistently using a quasilinear model and local approximation. We also explain the observed fast growth of electron cyclotron emission (ECE) signals and excitation of very low-frequency whistler modes observed in the quiescent RE experiments at DIII-D. Simulations using ITER parameters show that by controlling the background thermal plasma density and temperature, the plasma waves can also be excited spontaneously in tokamak disruptions and the avalanche generation of runaway electrons may be suppressed.

Introduction.- In a plasma, the collisional force decreases with increasing electron velocity and a strong electric field force can overcome the collisional damping, accelerating high energy electrons to relativistic speeds. Such electrons are referred to as "runaway electrons" (REs). In tokamaks, REs have attracted a lot of attention due to their deleterious effects on the device during disruption events[1, 2]. Studies of RE dynamics reveal that knock-on collisions can lead to avalanche multiplication of the RE population[3], and calculations show that the threshold electric field for this scenario, the Connor-Hastie field E_{CH}[4], is much smaller than the typical induced electric field in disruptions. Consequently, a strong RE avalanche effect could convert a large fraction of Ohmic current to RE current during disruptions. Aside from tokamak plasmas, RE avalanche is also important in other areas, such as lightning formation during thunderstorms[5].

Quiescent runaway electron experiments in well-controlled scenarios (called flattop) with low electron density have been conducted in several tokamaks[6–8]. The RE density and energy distributions have been inferred from radiation signals, including hard X-rays (HXR), gamma rays and electron cyclotron emission (ECE). An important finding in these experiments is that the value of the threshold electric field for the RE population to transition from growth to decay is not the expected E_{CH}[7, 9] but 5-10 times higher. This discrepancy with the theory indicates the presence of anomalous RE loss mechanisms, and numerical simulations have indicated the importance of radiative energy losses, including synchrotron[10, 11] and bremsstrahlung[12, 13]. However, theoretical calculations including these effects raise the threshold electric field to about 2 E_{CH}, which is still much smaller than that observed. In recent DIII-D experiments[14], the gamma-ray imaging (GRI) shows that the RE density decreases in the low energy regime while E remains several times E_{CH}, which differs from numerical simulation results including radiative losses. In addition, during both flattop[15] and the RE plateau in disruption experiments[16], strong ECE from REs was observed. These observations are suggestive of strong pitch angle scattering in the RE population at low energy, which could enhance radiative losses.

In this Letter, we demonstrate that a self-consistent kinetic treatment which includes the whistler-wave instability driven by the highly anisotropic RE momentum-space distribution provides a conclusive resolution of the observed discrepancy between theory and experiment. New simulations presented in this paper produce a threshold of $6.4E_{\mathrm{CH}}$, which is very close to observations.

Previous studies of kinetic instabilities associated with REs[17] have addressed the instability criterion[18], the diffusion effect on the electron distribution[19–22], and the convective aspect of the instabilities[23]. A detailed study containing also the avalanche effect and radiation damping is, however, missing. In the present work, we present a recently developed numerical model to study the evolution of both the runaway electron distribution and the wave energy spectrum self-consistently, including the avalanche source and the radiation reaction. The model includes the wave-particle interaction within the quasilinear approximation. Our numerical analysis of DIII-D flattop experiments and ITER post-disruption scenarios reveals that the whistler waves can enhance the avalanche for large $E/E_{\rm CH}$ (low density), but suppress the avalanche for small $E/E_{\rm CH}$ (high density). The results show an increase of the critical electric field and a rapid increase in the ECE from REs, also seen in the experiments.

Simulation framework.- The whistler wave belongs to the fast wave branch of the plasma wave dispersion relation. In this work, the frequency and the polarization of the whistler waves for every (k,θ) (with $\theta = \arccos k_\parallel/k$) are calculated using the cold plasma dielectric tensor. We also calculate the collisional damping rate according to the electron-ion collisional frequency[23].

The evolution of the electron distribution function f in momentum space is advanced through the kinetic equation. The coordinates for momentum space are (p,ξ), where p is the momentum normalized to mc (m is the electron mass and c is the speed of light), and $\xi = p_\parallel/p$. The kinetic equation we solve is[24]

$$\frac{\partial f}{\partial t} + \frac{eE_\parallel}{mc}\left(\xi\frac{\partial f}{\partial p} + \frac{1-\xi^2}{p}\frac{\partial f}{\partial \xi}\right) + C\left[f\right] + \frac{\partial}{\partial \mathbf{p}}\cdot\left(\mathbf{F}_{\rm rad} f\right) + D\left[f\right] = S_A\left[f\right], \tag{1}$$

with $E_\parallel$ the parallel electric field, $C[\dots]$ the collision operator[25, 26]. $\mathbf{F}_{\rm rad}$ is the synchrotron radiation reaction force term[11]. $D\left[\dots\right]$ is the diffusion operator from the excited waves. $S_A\left[\dots\right]$ is the source term for the avalanche[2, 27].

Given the distribution function, we can obtain the growth (or damping) rate Γ of every mode, using[23][28]

$$\Gamma(k,\theta) = \frac{\omega_{pe}^2}{\mathcal{D}}\int d^3p \sum_{n=-\infty}^{n=\infty} Q_n \pi\delta(\omega - k_\parallel v\xi - n\omega_{ce}/\gamma)(p^2/\gamma)\hat{L}f, \tag{2}$$

where

$$Q_n = \left[\frac{n\omega_{ce}}{\gamma k_\perp v}J_n(k_\perp\rho) + E_z\xi J_n(k_\perp\rho) + iE_y\sqrt{1-\xi^2}J_n'(k_\perp\rho)\right]^2, \tag{3}$$

$$\hat{L} = \frac{1}{p}\frac{\partial}{\partial p} - \frac{1}{p^2}\frac{n\omega_{ce}/\gamma - \omega(1-\xi^2)}{\omega\xi}\frac{\partial}{\partial \xi}, \tag{4}$$

Here ω_{pe} and ω_{ce} are the plasma frequency and electron cyclotron frequency (we choose $\omega_{ce} < 0$), J_n is the nth order Bessel function, v is the particle velocity, γ is the relativistic factor, and $\rho = mp\sqrt{1-\xi^2}/\omega_{ce}$ is the Larmor radius. $\mathcal{D}$ is from Eq. (21) in [23]. E_y and E_z are wave polarization normalized to E_x. f is normalized so that $\int p^2 dp d\xi f = 1$.

The wave energy $\mathcal{E}(k,\theta)$ then evolves as

$$\frac{d\mathcal{E}(k,\theta)}{dt} = 2\Gamma(k,\theta)\mathcal{E}(k,\theta) + \mathcal{K}(k,\theta), \tag{5}$$

where $\mathcal{K}(k,\theta)$ represents the fluctuation electromagnetic field energy from radiation, which provides the initial amplitudes of the modes[29]. $\mathcal{K}$ can be calculated as

$$\mathcal{K}(k,\theta) = \frac{\omega_{pe}^2}{\mathcal{D}}\int d^3p \sum_{n=-\infty}^{n=\infty} Q_n \pi\delta(\omega - k_\parallel v\xi - n\omega_{ce}/\gamma) m v^2 f. \tag{6}$$

The diffusion of resonant electrons can be calculated using a quasilinear diffusion model[30],

$$D[f] = \frac{e^2}{2\mathcal{D}}\sum_{n=-\infty}^{\infty}\int d^3\mathbf{k}\,\hat{L}\left[p_\perp \delta(\omega - k_\parallel v\xi - n\omega_{ce}/\gamma)\mathcal{E}(k,\theta)Q_n p_\perp \hat{L} f\right]. \tag{7}$$

Note that in Eqs. (2), (6) and (7), the wave-particle interaction happens only when the resonance condition is satisfied: $\omega - k_\parallel v\xi = n\omega_{ce}/\gamma$. This includes Cherenkov resonance ($n = 0$), normal Doppler resonance ($n < 0$) and anomalous Doppler resonance ($n > 0$). For anomalous Doppler resonance, the resonant momentum p is a decaying function of ω for a fixed θ, thus the low energy electron will resonate with high frequency waves and vice versa. For Cherenkov resonance, p is a non-monotonic function of k and θ, so for low frequency whistler waves (LFWWs) and high frequency whistler waves (HFWWs), the resonance regions overlap.

The numerical representation of f and $\mathcal{E}$ is adjusted, guided by the anticipated shape of the solution. For f, we use finite element method with 1000 elements in p and 50 elements in ξ. For $\mathcal{E}$, we use a mesh with 50 points in θ and 160 points in k. For every mode, we calculate a line integral for f to obtain Γ and $\mathcal{K}$ according to Eq. (2)(6). For the diffusion operator, we use linear interpolation to get the wave energy required by Eq. (7) for every quadrature point in the f mesh. In the calculation of Eqs. (2) and (7), we only include $n = 0, \pm 1$ assuming they are the most dominant resonances. The timestep is chosen

according to $\Delta t = 1/\Gamma_{\max}$, where $\Gamma_{\max}$ is the maximum value of Γ for all the modes. For every timestep, the evolution of $\mathcal{E}$ is calculated by integrating Eq. (5) for Δt.

To better validate against experiments, we also developed an ECE synthetic diagnostic code to calculate the ECE radiation power[29, 31, 32]. Note that in the current model we only have the electron distribution in 2D momentum space, thus to calculate the ECE signals, we assume that the electron distribution containing a runaway tail is homogeneous in space near the core from $-0.5a$ to $0.5a$ (a is the minor radius), and outside this region, the electron distribution is a Maxwellian distribution with a specified temperature profile.

Simulation of flattop RE experiment scenarios.- We now use the model to simulate a DIII-D flattop experiment[14], which has strong RE generation due to the avalanche process. Note that a typical RE discharge consists of two stages. In stage I, the plasma density is very low and the parallel electric field supporting the Ohmic current is sufficient to accelerate a RE tail. When the REs reach a critical intensity, an asynchronous trigger begins the RE dissipation stage, in which the electron density is varied by gas puffing. The parameters we use in simulation are close to the numbers from the tokamak core diagnostic. For stage I, $n_e = 0.6 \times 10^{19}\mathrm{m}^{-3}$, $T_e = 1.3\mathrm{keV}$, and $B = 1.45\mathrm{T}$. $E_\parallel = 0.055\mathrm{V/m}$, which is about $9E_{\mathrm{CH}}$. For stage II, we increase the density to $n_e = 0.8 \times 10^{19}$, by adding a Maxwellian part to f from the last timestep of stage I. We also decrease the electric field to $E = 0.045\mathrm{V/m}$, so E/E_{CH} becomes 5.5. The effective ion charge is set to be $Z_{\mathrm{eff}} = 2$ [14].

The simulation result of stage I is summarized in Fig. 1. Before 0.5s, the RE tail is formed through Dreicer generation (Fig. 1 (c)). In this case all the modes are stable. Then as the RE tail extends to $p = 15$, the LFWWs (from 1GHz to 5GHz, as shown in Fig. 1(d)) first get excited, due to the anomalous Doppler resonance with electrons at $p_\parallel > 15mc$. This gives rise to strong pitch angle scattering for high energy REs[17, 19] (as shown below in Fig. 2(a)).

After 1.6s, the HFWWs also get excited as shown in Fig. 1 (e) (the wave close to the spectrum right boundary which is the resonance cone). These waves resonate with lower energy electrons ($1.5 < p/mc < 4$) through anomalous Doppler resonance. The result of the excitation, as shown in Fig. 2(b), is that the low energy REs can be scattered to very large pitch angle. This effect also leads to the fast growth of the ECE signals. Calculation of ECE weight function[32] shows that electrons in the low energy regime with large pitch angle are the most efficient at generating ECE power. This explains why the ECE signals

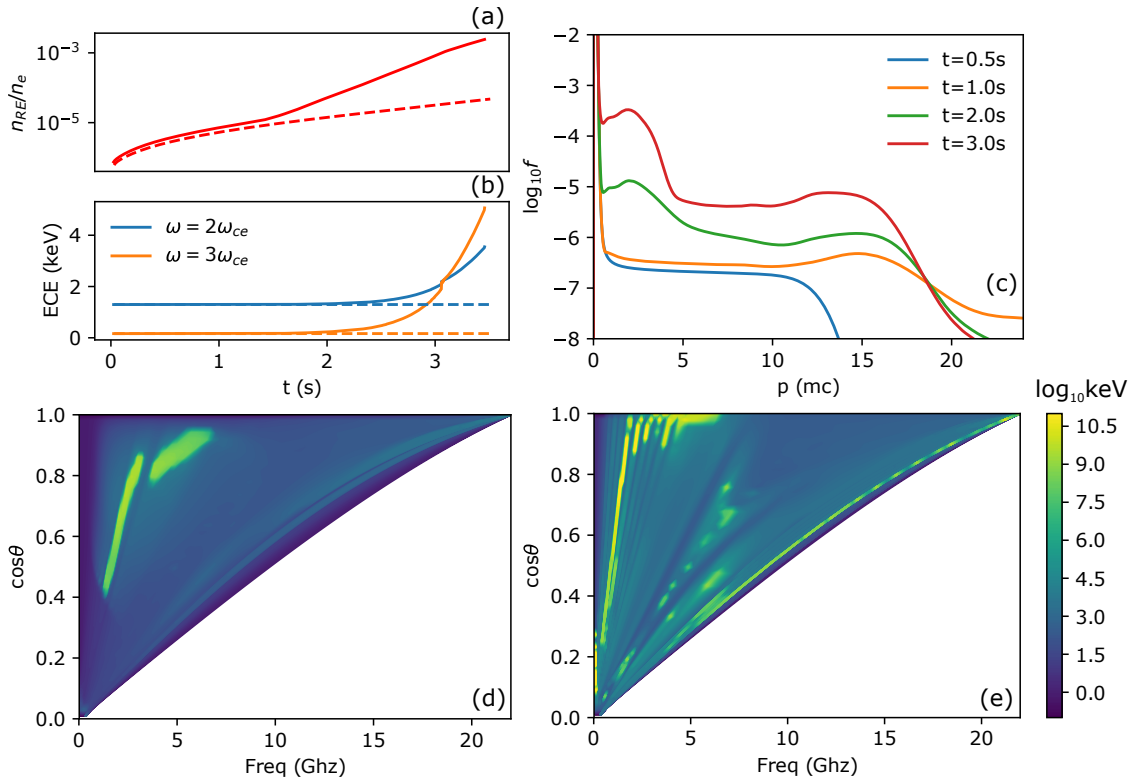

FIG. 1. (a) Growth of RE density with time, with wave diffusion (solid) and without (dashed). (b) ECE signals of second and third core ω_{ce}, with wave diffusion (solid) and without (dashed). (c) Evolution of f integrated over the pitch angle. (d) Whistler wave energy spectrum for $t = 1.0$s. Right boundary is the whistler wave resonance cone. (e) Whistler wave energy spectrum for $t = 3.0$s.

only start to grow after the HFWWs get excited. We also observe that the higher frequency ECE signal surpasses the lower frequency one, which agrees with experiments[15].

As shown in Fig. 1 (a), after the HFWWs are excited, the avalanche growth rate increases. This effect is caused by diffusion of electrons in momentum space through Cherenkov resonance. Using the resonance condition, we find that the Cherenkov resonance region for the excited waves is about $0.4 < v_\parallel/c < 0.6$, which is close to the runaway-loss separatrix[33] in this case ($0.3 < v_\parallel/c < 0.5$ for $\xi = 1$). Note that the electron distribution function close to the separatrix satisfies $\partial f/\partial p_\parallel < 0$, so diffusion makes low energy electrons move to higher energy, and make them more prone to "run away".

We now look at stage II, which is shown in Fig. 3. According to the previous theories[11, 34], the electric field is still larger than the critical electric field, so the runaway population

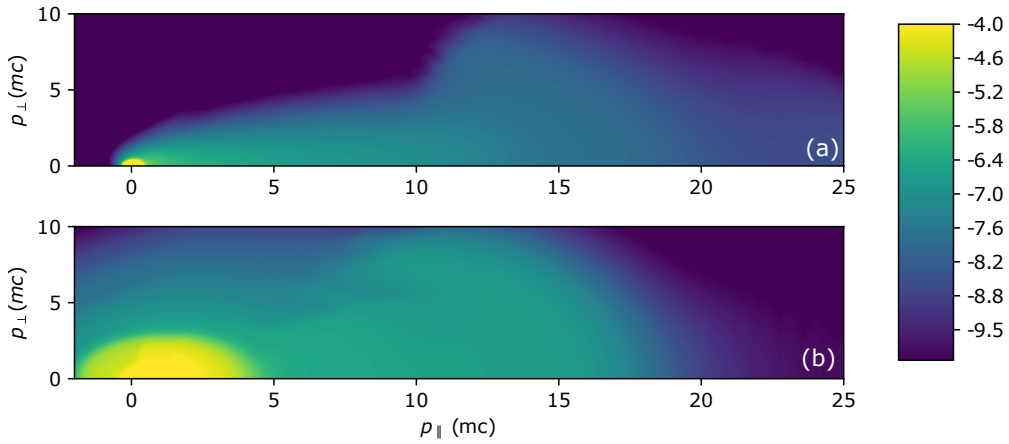

FIG. 2. (a) Value of $\log_{10} f$ in $p_\parallel - p_\perp$ space at $t = 1.0$s. (b) Value of $\log_{10} f$ in at $t = 3.0$s.

would grow if this were the extent of the model. This is confirmed in our simulation without wave diffusion, as shown by the dashed line in Fig. 3 (a). However, with the wave diffusion, the RE population actually starts to decay. Examination of the evolution of f (Fig. 3 (c)) reveals that this is caused by the loss of the REs in the lower energy regime, which is in agreement with recent findings in DIII-D[14]. The whistler wave spectrum and the shape of RE distribution function in stage II is similar to those of the later phase of stage I.

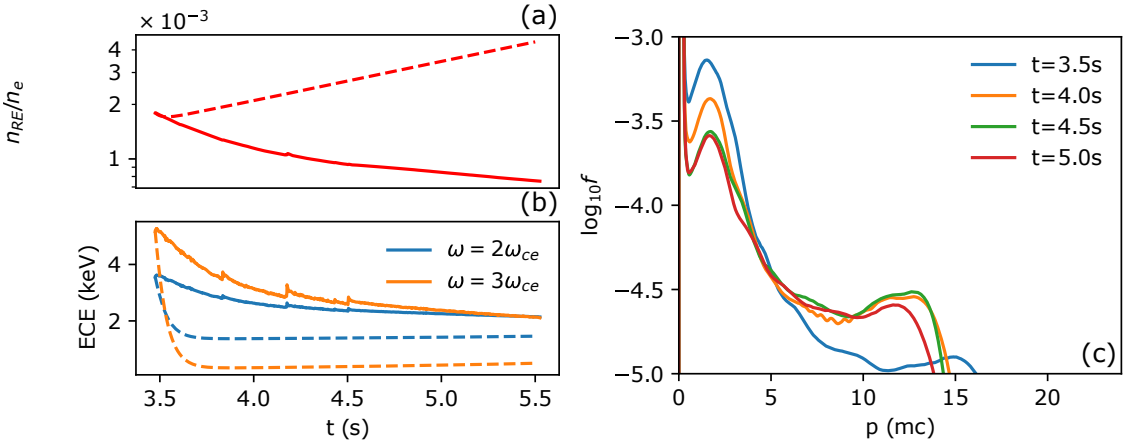

FIG. 3. (a) Evolution of RE density, with wave diffusion (solid) and without (dashed). (b) ECE signals with wave diffusion (solid) and without (dashed). (c) Evolution of f integrated over pitch angle.

The fact that the RE population decays because of wave diffusion seemingly contradicts

the results from stage I. This is because the diffusion effects from HFWWs can scatter REs to large pitch angles in the low energy regime through anomalous Doppler resonance, which become less susceptible to the electric force acceleration and can more easily lose energy. This mechanism provides a new channel for RE loss. In addition, in stage II the runaway-loss separatrix is at $0.5 < v_{\parallel}/c < 0.7$, due to the reduction of $E/E_{\rm CH}$, which does not overlaps with the Cherenkov resonance region. So the diffusion across the separatrix is less significant.

The effect of wave diffusion in momentum space is further illustrated in Fig. 4 (a), where we show the directions of flux in momentum space calculated from the kinetic equation. In the high energy regime, a vortex structure is formed ($10 < p_{\parallel} < 15$) due to LFWWs. The location of the vortex is in a much lower energy than that from radiation forces[35]. This vortex can hinder REs from going into the higher energy, resulting in a bump-on-tail distribution. On the other hand, in the low energy regime ($-5 < p_{\parallel} < 3$) electron flux is stochastic since the dynamics are dominated by diffusion rather than advection. The strong diffusion in this region comes from both LFWWs and HFWWs through all three types of resonances. Electrons entering this region can be diffused from low pitch angle to high pitch angle, losing energy to the waves, and finally returning to the thermal population.

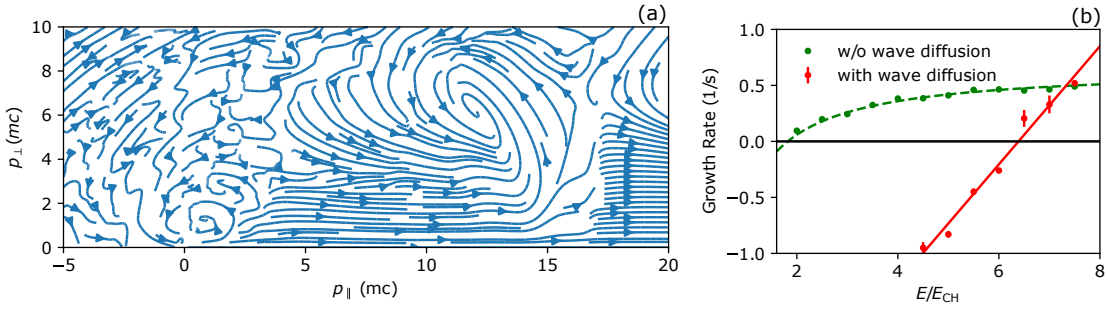

FIG. 4. (a) Electron flux in momentum space at $t = 4.0$s. (b) RE density growth (decay) rate as a function of $E/E_{\rm CH}$. The red dots are from the simulations with wave diffusion, and the red line is a linear regression. The green dots are from the simulations without wave diffusion, and the green dashed line is the growth rate calculated from [3], with critical electric field $E_{\rm c} = 1.82E_{\rm CH}$ from [27]

The decay of RE density in stage II indicates that the excitation of whistler waves can increase the critical electric field. Scanning n_e keeping other parameters fixed shows that the

new critical electric field is about $E/E_{\rm CH} = 6.4$ (Fig. 4 (b)). This value is much larger than the previous predictions with radiation reaction but without kinetic instabilities[36] (Green line in Fig. 4 (b)), and is closer to the experimental observation[37]. For $E/E_{\rm CH} \lesssim 6.4$, the avalanche is suppressed by whistler waves due to the anomalous Doppler resonance scattering. But for $E/E_{\rm CH} \gg 6.4$, the avalanche is enhanced because of Cherenkov resonance diffusion across separatrix.

We also use our numerical model to study the excitation of recently observed very low frequency whistler waves[38]. By examining the whistler wave spectrum in stage II, we find that a branch of whistler modes with frequency between 100MHz to 200MHz and $k_\perp \gg k_\parallel$ are excited in our simulation. Unlike previously discussed waves, these waves are mainly driven by the Cherenkov resonance. This is because the low-energy REs scattered by HFWWs can accumulate in a region of momentum space, which can cause an unstable bump-on-tail distribution function. This is illustrated in Fig. 4 (a), where we see electrons on the left side of the vortex ($p_\parallel \sim 5mc$, $p_\perp > 8mc$) losing $p_\parallel$ due to interaction with waves.

Note that in the local analysis of kinetic instabilities presented so far, we didn't take into account for the finite spatial extent of excited waves, termed the convective effect[23, 39]. To understand it, we use a ray tracing code GENRAY[40] to study the propagation of the whistler waves. We find that, for both LFWWs and HFWWs excited in our simulations, the rays will have trajectories bouncing back and forth in the poloidal plane, and the values of $n_\parallel$ and $n_\perp$ will stay close to their initial values when the wave packet propagates near the core[41]. This means that the resonance conditions of these waves will not be qualitatively different from that obtained from local analysis, but the growth rates may be overestimated by a few times.

In addition to flattop experiments, we also study the kinetic instabilities in disruptions. However, we find that for typical post-disruption parameters of ITER, kinetic instabilities can hardly be excited due to strong collisional damping at low temperature ($\sim$ 5eV). On the other hand, if we use a lower density ($n_e = 2 \times 10^{19}\mathrm{m}^{-3}$) and raise the electron temperature to about 50eV, we find that both LFWWs and HFWWs can be excited. This density and temperature thresholds are consistent with previous estimations[23, 39]. With kinetic instabilities, we find the avalanche growth can be enhanced for large $E/E_{\rm CH}$ but suppressed for small $E/E_{\rm CH}$, and the critical electric field is larger than what classical theory predicts. Note that in disruption experiments with possible higher temperature[16], signals of kinetic

instabilities have been observed. This suggests that in order to excite whistler waves and mitigate the avalanche, it may be beneficial to reduce the thermal electron density by injecting low-Z particles, and increase the thermal plasma temperature using external heating techniques. However, for post-disruption scenarios the presented work on the effect of the kinetic instabilities is preliminary due to the lack of orbit effect of electrons and convective effects of waves, and a more dedicated and systematic study should be performed in the future.

Summary.- To conclude, with the help of a new simulation model, we have advanced our understanding of the interactions of kinetic instabilities and RE avalanche. We find that for both flattop and post-disruption cases, the excited kinetic instabilities can enhance the avalanche growth for large E/E_{CH} but suppress it for low E/E_{CH}. The RE distribution function in momentum space, taking into account wave diffusion, differs significantly from the classical runaway electron tail, prompting a qualitative revision of earlier theoretical studies. Using this model, we successfully explain several phenomena in DIII-D flattop RE experiments after gas puffing, including 1) the increase of the critical electric field, 2) the decaying of RE density in the low energy regime, 3) the ECE from runaway electrons, 4) the observation of very low frequency whistler waves. These results suggest the possibility of controlling RE avalanche through kinetic instabilities, including both self-generation and external wave-launching[42]. The simulation model can be improved by including radial transport of REs due to stochastic magnetic fields, and the pitch angle scattering due to impurities[43].

Chang Liu would like to to thank Tünde Fülöp, Gergo Pokol, Allen Boozer, Boris Breizman, Lei Shi, Nicola Bertelli, Richard Harvey, Donald Spong and William Heidbrink for fruitful discussions. This work has received funding from the Department of Energy under Grant No. DE-SC0016268 and DE-AC02-09CH11466.

[1] H. Knoepfel and D. A. Spong, Nucl. Fusion **19**, 785 (1979).

[2] A. H. Boozer, Phys. Plasmas **22**, 032504 (2015).

[3] M. N. Rosenbluth and S. V. Putvinski, Nucl. Fusion **37**, 1355 (1997).

[4] J. W. Connor and R. J. Hastie, Nucl. Fusion **15**, 415 (1975).

[5] A. V. Gurevich, G. M. Milikh, and R. Roussel-Dupre, Phys. Lett. A **165**, 463 (1992).

[6] G. Fussmann, D. Campbell, A. Eberhagen, W. Engelhardt, F. Karger, M. Keilhacker, O. Klüber, K. Lackner, S. Sesnic, F. Wagner, K. Behringer, O. Gehre, J. Gernhardt, E. Glock, G. Haas, M. Kornherr, G. Lisitano, H. M. Mayer, D. Meisel, R. Müller, H. Murmann, H. Niedermeyer, W. Poschenrieder, H. Rapp, N. Ruhs, F. Schneider, G. Siller, and K. H. Steuer, Phys. Rev. Lett. **47**, 1004 (1981).

[7] C. Paz-Soldan, N. W. Eidietis, R. Granetz, E. M. Hollmann, R. A. Moyer, J. C. Wesley, J. Zhang, M. E. Austin, N. A. Crocker, A. Wingen, and Y. Zhu, Phys. Plasmas **21**, 022514 (2014).

[8] R. J. Zhou, L. Q. Hu, E. Z. Li, M. Xu, G. Q. Zhong, L. Q. Xu, S. Y. Lin, J. Z. Zhang, and t. E. Team, Plasma Phys. Control. Fusion **55**, 055006 (2013).

[9] R. S. Granetz, B. Esposito, J. H. Kim, R. Koslowski, M. Lehnen, J. R. Martin-Solis, C. Paz-Soldan, T. Rhee, J. C. Wesley, L. Zeng, and I. M. Group, Phys. Plasmas **21**, 072506 (2014).

[10] F. Andersson, P. Helander, and L.-G. Eriksson, Phys. Plasmas **8**, 5221 (2001).

[11] A. Stahl, E. Hirvijoki, J. Decker, O. Embréus, and T. Fülöp, Phys. Rev. Lett. **114**, 115002 (2015).

[12] M. Bakhtiari, G. J. Kramer, M. Takechi, H. Tamai, Y. Miura, Y. Kusama, and Y. Kamada, Phys. Rev. Lett. **94**, 215003 (2005).

[13] O. Embréus, A. Stahl, and T. Fülöp, New J. Phys. **18**, 093023 (2016).

[14] C. Paz-Soldan, C. M. Cooper, P. Aleynikov, D. C. Pace, N. W. Eidietis, D. P. Brennan, R. S. Granetz, E. M. Hollmann, C. Liu, A. Lvovskiy, R. A. Moyer, and D. Shiraki, Phys. Rev. Lett. **118**, 255002 (2017).

[15] C. Paz-Soldan, R. J. L. Haye, D. Shiraki, R. J. Buttery, N. W. Eidietis, E. M. Hollmann, R. A. Moyer, J.E. Boom, I. T. Chapman, and J. E. T. Contributors, Nucl. Fusion **56**, 056010 (2016).

[16] E. D. Fredrickson, M. G. Bell, G. Taylor, and S. S. Medley, Nucl. Fusion **55**, 013006 (2015).

[17] V. V. Parail and O. P. Pogutse, Nucl. Fusion **18**, 303 (1978).

[18] T. Fülöp, G. Pokol, P. Helander, and M. Lisak, Phys. Plasmas **13**, 062506 (2006).

[19] G. Pokol, T. Fülöp, and M. Lisak, Plasma Phys. Control. Fusion **50**, 045003 (2008).

[20] A. Kómár, G. I. Pokol, and T. Fülöp, J. Phys.: Conf. Ser. **401**, 012012 (2012).

[21] G. I. Pokol, A. Kómár, A. Budai, A. Stahl, and T. Fülöp, Phys. Plasmas **21**, 102503 (2014).

[22] A. Kómár, G. I. Pokol, and T. Fülöp, Phys. Plasmas **20**, 012117 (2013).

[23] P. Aleynikov and B. Breizman, Nucl. Fusion **55**, 043014 (2015).

[24] See Supplemental Material at [URL] for expressions of the terms in the kinetic equation, which includes Refs. [44–47].

[25] P. Sandquist, S. E. Sharapov, P. Helander, and M. Lisak, Phys. Plasmas **13**, 072108 (2006).

[26] M. Landreman, A. Stahl, and T. Fülöp, Comput. Phys. Commun. **185**, 847 (2014).

[27] C. Liu, D. P. Brennan, A. H. Boozer, and A. Bhattacharjee, Plasma Phys. Control. Fusion **59**, 024003 (2017).

[28] Spatial gradient is ignored here given the wavelength is much smaller compared to spatial gradient scale length.

[29] R. W. Harvey, M. R. O'Brien, V. V. Rozhdestvensky, T. C. Luce, M. G. McCoy, and G. D. Kerbel, Physics of Fluids B: Plasma Physics **5**, 446 (1993).

[30] A. N. Kaufman, Physics of Fluids **15**, 1063 (1972).

[31] C. Liu, *Runaway electrons in tokamaks*, Ph.D. thesis, Princeton University (2017).

[32] C. Liu, L. Shi, E. Hirvijoki, D. P. Brennan, A. Bhattacharjee, C. Paz-Soldan, and M. E. Austin, arXiv:1803.09897 (2018).

[33] C. Liu, D. P. Brennan, A. Bhattacharjee, and A. H. Boozer, Phys. Plasmas **23**, 010702 (2016).

[34] P. Aleynikov and B. N. Breizman, Phys. Rev. Lett. **114**, 155001 (2015).

[35] Z. Guo, C. J. McDevitt, and X.-Z. Tang, Plasma Phys. Control. Fusion **59**, 044003 (2017).

[36] J. R. Martín-Solís, A. Loarte, and M. Lehnen, Nucl. Fusion **57**, 066025 (2017).

[37] C. Paz-Soldan, C. M. Cooper, P. Aleynikov, N. W. Eidietis, A. Lvovskiy, D. C. Pace, D. P. Brennan, E. M. Hollmann, C. Liu, R. A. Moyer, and D. Shiraki, Phys. Plasmas **25**, 056105 (2018).

[38] D. A. Spong, W. W. Heidbrink, C. Paz-Soldan, X. D. Du, K. E. Thome, M. A. Van Zeeland, C. Collins, A. Lvovskiy, R. A. Moyer, M. E. Austin, D. P. Brennan, C. Liu, E. F. Jaeger, and C. Lau, Phys. Rev. Lett. **120**, 155002 (2018).

[39] B. N. Breizman and P. B. Aleynikov, Nucl. Fusion **57**, 125002 (2017).

[40] A. Smirnov, R. Harvey, and K. Kupfer, in *Bull Amer. Phys. Soc.*, Vol. 39 (American Physical Society, 1994) p. 1626.

[41] See Supplemental Material at [URL] for the ray-tracing results.

[42] Z. Guo, C. J. McDevitt, and X.-Z. Tang, Phys. Plasmas **25**, 032504 (2018).

[43] L. Hesslow, O. Embréus, A. Stahl, T. C. DuBois, G. Papp, S. L. Newton, and T. Fülöp, Phys. Rev. Lett. **118**, 255001 (2017).

[44] S. C. Chiu, M. N. Rosenbluth, R. W. Harvey, and V. S. Chan, Nucl. Fusion **38**, 1711 (1998).

[45] O. Embréus, A. Stahl, and T. Fülöp, J. Plasma Phys. **84**, 905840102 (2018).

[46] C. Møller, Ann. Phys. **406**, 531 (1932).

[47] A. Ashkin, L. A. Page, and W. M. Woodward, Phys. Rev. **94**, 357 (1954).